Novel Technique for Meniscus Height Measurement of Liquids Using Optical Fibers

Leonardo Binetti and Lourdes S. M. Alwis

***Abstract*—A novel technique was designed to measure the meniscus height (MH) of liquids on a standard single mode fiber (SMF) using fiber optics. Once the MH is known, the contact angle could be calculated, and the surface tension of liquids can be determined. In this paper, the MH is measured using a cleaved and side polished optical fiber attached to a SMF with a known separation distance between their fiber tips. When the liquid reaches the SMF, the liquid meniscus rises on the vertical wall of the SMF, which also causes a variation in mass (measured by a µg scale). At this point, the liquid moves upwards until the liquid meniscus touches the side polished fiber, which registers a variation of the reflected optical power. The MH seems to increase as the surface tension decreases, and the variation of the mass measured by the scale increase with the increase of the surface tension. This sensor was also used to measure the interfacial surface tension of the air-liquid and liquid-liquid interface since the contact angle could be measured. In addition, the small dimension of the sensor is adequate for applications where using small amounts of liquid is critical, i.e., biomedical applications.**

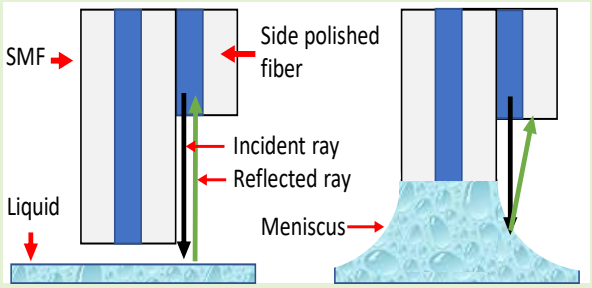

Index Terms—Contact Angle, Interfacial Surface Tension, Meniscus Height, Optical Fiber Sensor, Side Polished Fiber, Surface Tension.

I. Introduction

THE MEASUREMENT of surface tension in liquid is important in many industrial applications. For example, in the biomedical industry, an increase of surface tension within alveoli promotes the most severe manifestation of Covid-19 pneumonia, which decreases the gas exchange in the lung [1]. In addition, a decrease of surface tension in urine could be detrimental for diabetes patients [2]. Therefore, a variation in the surface tension value is correlated to the presence of diseases. Many apparatus have been developed during the last century to measure and quantify surface and interface forces of liquids [3]. Typical devices rely on immersing a solid into a liquid of interest to determine the macroscopic contact line between the solid and liquid (the wetted perimeter). The added force on the solid sample is the measured surface tension, which is then divided by the wetted perimeter. Among many different methods, the du Nuoy ring and the Wilhelmy plate methods are the most used tensiometers for air-liquid and liquid-liquid interface [3]. The former needs a meniscus correction factor since the size and geometry of the inside and outside surface of the ring are not comparable. The second needs a correction to determine whether the plate is partially or completely submerged in the liquid [3]. However, these techniques assume that the liquid curvature does not govern the surface tension, the liquid does not put on added forces to the submerged portion of the solid, the angle at the interface between the liquid and the vertical sample is known, and it is also assumed to be zero for receding contact angle [4]. However, the contemporary knowledge of both the contact angle and the surface tension of the liquid is an enormous limitation in this method.

Polynomial and other mathematical functions have been deployed to measure the value of the contact angle of the meniscus. However, errors in the mathematical function approximations used for static and dynamic contact angle measurements are still present [5]. Also, image processing contains errors. For example, to construct an image of the meniscus (especially with thin fibers), the correct number of pixels is needed, and a small change can affect the final result [6]. Another major concern of the Wilhelmy method is using a platinum plate (known for its high wettability). As a result, when measuring the surface tension of protein solutions, the plate becomes hydrophobic due to their adsorption onto the plate. Therefore, it is difficult to establish a zero contact angle between the plate and the liquid [7]. In addition, the assumption of zero contact angle is more difficult when the plate is at the interface between two liquids, often found in biological processes [8].

Optical Fiber sensors have been demonstrated to be extremely attractive because of their immunity to

Submission date for the review:20/04/2021

L. Binetti and L. S. M. Alwis are with the Edinburgh Napier University (e-mail: l.binetti@napier.ac.uk, l.alwis@napier.ac.uk)

electromagnetic interference, resistance to chemicals (which is superior to most metals and polymers [9]), and their small size [10]. Surface tension measurement, by optical fiber, was previously conducted either through the analysis of the optical path of the liquid on the optical fiber tip [11] or by measuring the lateral force [12]. However, besides problems of alignment and difficult calculation for the first, high amount of liquid and the use of expensive optical fiber (tilted fiber Bragg grating (TFBG) in transmission) for the second, they both need to use expensive cameras to detect the contact angle, and as mentioned above, the image processing is not accurate to an acceptable level [13].

In the work presented here, a side polished single mode fiber (SMF) is cleaved and interrogated in reflection mode. This fiber was attached to a standard SMF and used as a contact angle reader. The Wilhelmy method was modified to obtain the contact angle by measuring the meniscus height (MH) on the standard SMF. In addition, the force of the liquid on the fiber is measured with a µg sensitive scale. Furthermore, the diameter of the optical fiber is 125 µm, which provides considerable advantages, in terms of its physical dimensions, compared to a plate. Moreover, steady-state measurements are possible with high viscosity liquids, and higher accuracy results are possible due to the rapid equilibration of the *MH* on a relatively small and stationary optical fiber [14]. Besides, once the meniscus forms on the standard SMF, it rises on the optical fiber wall and reaches the equilibrium height within tens of milliseconds. This amount of time is five times less than on a capillary tube [15][16]. Finally, the optical fiber-based system presented here measures the contact angle at the interface between two liquids while decreasing the volume of the liquid sample required [17].

II. Methodology

A. Materials

The following chemicals used were of analytical grade, and no other purifications were conducted. Acetone 99%, isopropanol 99.7 % (IPA), glycerol ≥ 99.5 %, diiodomethane 99%, and ethylene glycol ≥ 99 %, were purchased from Sigma Aldrich UK. Water extra pure, deionized was acquired from Acros Organics. P3 mineral oil was purchased from Pfeiffer Vacuum. In this paper, the optical fiber was of standard grade (ITU G.652.D).

B. Static surface tension measurement

In the Wilhelmy method, the system experiences an increase or decrease in weight as the surface tension attracts or pushes the plate (if the contact angle between the solid and liquid at the solid-liquid interface is less or higher than 90°, respectively). The Archimedes' force acts on the plate too, pushing the dipped part. Thus, the equation describing the total force (F_{Tot}) that the plate experiences depends on the capillary (*Fc)*, the buoyancy (F_B), and gravitational (F_G) forces. The gravitational force is equal to zero if the tensiometer is zeroed to a point very close to the surface of the liquid. In the case of a small optical fiber, the buoyancy force is negligible, especially for a diameter *d* in the range between 20 and 300 µm [18]. Thus, the surface tension depends solely on the capillary force and is given by [18],

$$F_{Tot} = \pi \cdot d \cdot \gamma \cdot cos\theta = g \cdot m_S \quad (1)$$

where m_S is the wetting mass on a stationary fiber, γ is the surface tension, θ is the contact angle, and g is the acceleration due to gravity. A requirement of the Wilhelmy method is ensuring an even cross-section of the object that is to be immersed in the liquid so that the wetting perimeter is stable [19]. If the fiber presents an irregular surface, the meniscus height would present different measurements at micro-level. Therefore, the fiber was carefully cleaved, which also avoid any irregularities that may hinder an adequate Fabry-Perot interference. Considering that the diameter of the fiber is 125 µm, the contact angle is 0°, and the surface tension of water is 72.8 mN/m, a F_{Tot} on the silica optical fiber is calculated to be ~28.6 µN; thus, a force in the µN range is expected. The variation of the added mass on the cleaved optical fiber was measured with a highly sensitive scale (Radwag MYA 5 with a sensitivity of 1 µg). Following this, the fiber was immersed in a detergent cleaning solution, then acetone, consequently in deionized water, and was dried at room temperature. The optical fiber was connected to the laser interrogator unit (Micron Optic sm125), and the reflected optical spectrum was recorded in the air with the manufacturer-provided software Enlight©. When the fiber is in contact with the liquid, a variation in optical reflected power is observed [17]. Consequently, the whole system was moved toward the liquid until the scale registered a mass variation. The speed of motion was 0.1 mm/min, thanks to the use of Lloyd Instruments (QA LRX 05).

C. Static contact angle measurement

To calculate the static contact angle on the cleaved SMF from (1), the static *MH* must be known. For this reason, James' asymptotic equation was used [20] as follows,

$$MH \sim r sin\Phi \left\{ ln\left[\frac{4}{\beta(1+cos\Phi)}\right] - \kappa \right\} for\ \beta \to 0 \quad (3)$$

where β is the Bond number ($\beta^2 = \rho g r^2/\gamma$), κ is the Euler's constant, which is approximately 0.58 [21][22], ρ is the density, and r is the radius of the optical fiber and $\Phi = \frac{\pi}{2} - \theta$. Since β is less than 0.1 for the selected liquids (see Table I), the error associated to James' formula is negligible [23].

D. Fabrication of the side polished fiber

A cleaved and side polished fiber was fabricated for the static contact angle measurement, as shown in Fig. 1. A microscope

analysis (with Olympus BX53M) was conducted on the cleaved region to evaluate the quality of the cleave. In addition, the reflected optical power spectrum of the bare optical fiber (Fig. 1(a)) in the air was registered using the interrogator (between 1520 and 1580 nm). Subsequently, the fiber is placed onto a plastic mold, and the cross-sectional area of the cleaved SMF tip was covered with adhesive tape. In this case, the tape protects the cleaved end from the liquid mounting resin poured on the optical fiber end. The resin is composed of the mixture of one part of the quick set mounting liquid (MetPrep REF 111036) and two parts of powder (MetPrep REF 111035). In addition, once the resin is set, it provides mechanical strength and stability to the side polished fiber. Then the optical fiber (with the resin) was removed from the plastic mold, the tape removed, the optical fiber tip was immersed in IPA (to clean any tape residues), and successively immersed in water until the reflected optical power spectrum resumed to that of the cleaved optical fiber in the air once the optical fiber tip was dried. The mounted optical fiber was then ground and polished, see Fig. 1(b), using an automated grinding machine (Struers TegraPol-21) from 16 to 1 µm, offering a satisfactory surface finish. The optical fiber was closely monitored at each stage using the microscope until a certain degree of polishing length (55.0, 59.0, and 61.0 µm) of the cleaved optical fiber was achieved, while the reflected optical power was also simultaneously monitored. With a polished side length of 59.0 and 61.0 µm, a variation in the reflected optical power was also observed due to the access of the optical fiber core. In this case, it was observed that the side polished fiber could also measure the reflected optical power variation on the polished side.

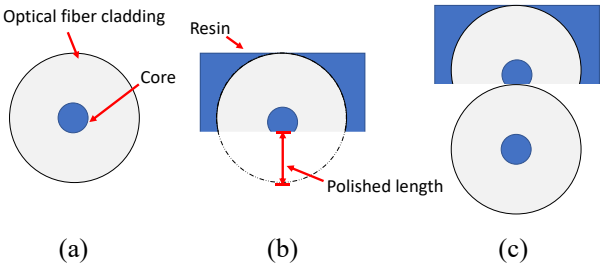

Fig. 1. Cross sectional view of the bare (a) side polished fiber (b), and end-face, i.e., the tip, view of the fiber setup when the polished and bare fiber is attached together (c).

Once the fiber was polished, it was attached to a cleaved bare SMF. This attachment, in which the end-face of both fibers, i.e., the tip, is shown in Fig. 1(c), was obtained by first using a clamp, and the distance *D* from the fiber tip was adjusted, as shown in Fig. 2(a). Then the two fibers were secured with cyanoacrylate glue. The attachment was carefully inspected using the microscope to ensure no gap, i.e., air, between the two fibers. Also, the tip of the fiber was carefully monitored for any contamination, i.e., to avoid any residue glue being present. This setup was passed through a 3D printed hole made in the lid of a beaker so that the evaporation of the liquid was minimized. Before each analysis, the two optical fibers were inserted in the beaker, i.e., containing the liquid under analysis, and kept for two hours to ensure that the vapor was in equilibrium with both its liquid and with the solid [24], i.e., the optical fiber. The liquid was then moved upwards towards the optical fibers, as shown in Fig. 2(b). When the meniscus of the liquid forms on the vertical edge of the SMF, a reflected optical power variation is registered. From this point, the displacement is recorded until the side polished fiber registers the spectrum of the liquid (the spectrum was registered at small steps of 0.833 µm traveled distance for 0.5 seconds to increase the precision of the measurement), as shown from Fig. 2(c) to Fig. 2(d). The displacement is subtracted by the initial distance *D*, which provides the measurement of the *MH*.

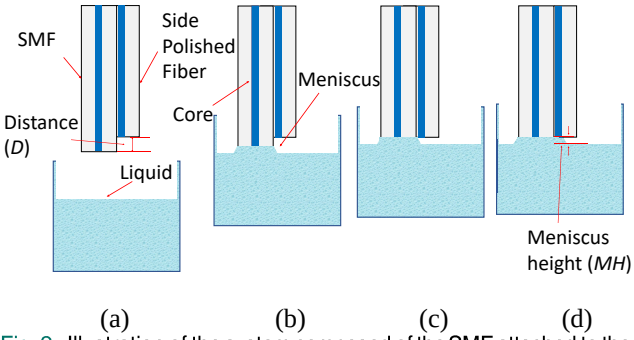

Fig. 2. Illustration of the system composed of the SMF attached to the side polished fiber, with a known distance D (a). When the side polished fiber approaches the liquid, the meniscus forms initially on the SMF (b) and then reaches the side polished fiber (c). Eventually, the liquid covers the core of the polished fiber (d).

E. Surface Energy and AFM analysis

The surface energy of the optical fiber was calculated using the Van Oss-Chaudhury-Good method, mostly used for high polar surfaces like glass [25]. This method considers that the solid surface is composed of non-polar and polar sites by measuring the contact angle (in the case presented here, through the *MH*) on the optical fiber. The contact angle of the non-polar sites is measured by immersing the optical fiber in diiodomethane since it presents non-polar components. For the polar components, which are acid and base (from Lewis's theory), the contact angle of the optical fiber is measured with deionized water and ethylene glycol. Since the surface energy depends on the morphology of solids [16], morphological analysis has been done on the SMF, with an atomic force microscope AFM (Veeco Explorer).

F. Interfacial surface tension

As described before, the Wilhelmy method cannot measure the interfacial surface tension between two liquids. This is because the contact angle is not guaranteed to be 0° when the plate or optical fiber is between two liquids. Hence, the interfacial surface tension between the mineral oil and deionized water has been measured using the same principle

used for air-liquid interface by measuring the difference in weight from the scale and the contact angle with the side polished fiber. In addition, the estimation of the theoretical liquid-liquid surface tension was obtained using Young's equation:

$$\gamma_{L2} = \gamma_{L1,L2} + \gamma_{L1}\cos\theta \quad (4)$$

where γ_{L1}, and γ_{L2}, are the surface tension of the first and second liquid, $\gamma_{L1,L2}$ is the interfacial surface tension between the two liquids.

G. Evaporation correction

The rate of evaporation of a liquid, increases when the meniscus forms on a solid [24]. Thus, for this reason, the measurement of the evaporation rate is needed to ensure correct measurement. The rate of evaporation was measured, for this specific case, with a bare SMF that registers the variation of the reflected optical power when the fiber tip is in contact with the liquid. After 10 min, the optical fiber was removed from the liquid, and the distance for the optical fiber to be in contact again with the liquid was used to detect the evaporation rate. The re-immersion of the fiber was carried out after a one-minute wait, giving adequate time for the evaporation of the droplet of liquid to form on the fiber end. With this procedure, the possible error associated with the presence of liquid at the fiber tip was avoided.

TABLE I
CHEMICAL PROPERTIES

Liquid	Density (kg/m^3)	β (10^{-2})	Surface tension (mN/m)
Deionized Water	997	2.2	72.8
Glycerol	1126	2.6	64.0
Diiodomethane	3320	5.0	50.8
Ethylene Glycol	1097	3.0	48.0
Mineral Oil	870	3.5	28.0
Acetone	791	3.6	23.0
IPA	785	3.8	20.9

III. RESULT AND DISCUSSION

A. Force Measurement

As mentioned in the methodology section, the force on the cleaved optical fiber was measured by detecting the variation in mass with a sensitive scale. As shown in Fig. 3, the variation of mass due to the surface tension properties of the selected liquids shows a linear relationship as shown in [26]. In the case of water, the force registered is lower than ~28.6 μN, which indicates that the contact angle between water and the fused silica of the cladding material of the optical fiber is not 0°. Therefore, the contact angle via the *MH* needs to be measured, as described in the next sections.

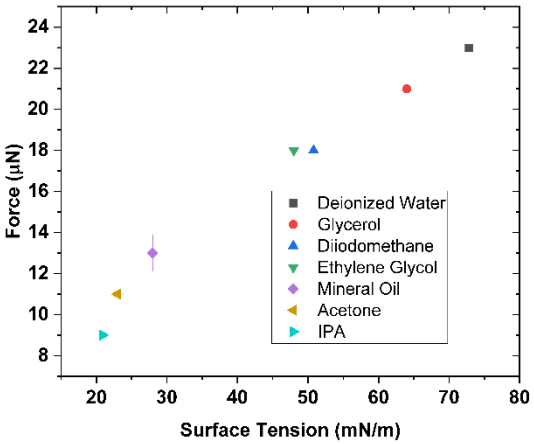

Fig. 3. Force, measured by the scale, as the surface tension of the liquid changes.

B. Evaporation rate

Before measuring the *MH*, the measurement of the evaporation rate is needed. As mentioned in the methodology section, an evaporation correction was applied to the *MH* results, especially for acetone, which has the highest volatility compared to the other liquids in Table I. However, after two hours, the evaporation rate for acetone was constant at 6.6 ± 0.3 μm/min. For this reason, all liquids were kept in their beaker for at least two hours before the start of the measurement.

C. Side polished fiber

In order to measure the surface tension of a liquid, besides the measured force, the value of the contact angle is needed, as shown in (1). Thus, side polished fiber with different polished lengths (55, 59, and 61 μm) was produced. A decrease in the reflected optical power was noticed as the side polished length increased from 55 to 61 μm, as expected since the core of the optical fiber was further exposed. A variation of the reflected optical power between the bare SMF and the side polished fiber before reaching the liquid surface is present in Fig. 4(a). In this case, the SMF average reflected power is at about -23 dBm, whereas the average reflected power of the side polished fiber lies at approximately -26 dBm. The discussion on the interference pattern is presented in the next paragraph.

The side polished fiber was attached to a bare SMF for the contact angle measurement, with a fixed distance *D* between their cleaved fiber tip, as shown in Fig. 2. The distance *D*, measured with the microscope, was 400.0 ± 0.1 μm. This particular distance was chosen so that it was longer than the vertical height of the meniscus would form on the SMF. In Fig. 4(a), the period of the interferometric oscillation before the liquid reaches the fiber is shown. This period is larger for the bare SMF since it is closer to the liquid surface. In comparison, the side polished fiber, which is at a longer distance from the

liquid surface, presents a smaller interferometric period of its reflected optical power.

Once the liquid reaches the cleaved end of the SMF, its reflected optical power decreases (see Fig.4(a)) due to the change in refractive index, i.e., from air to that of the liquid (see Table II). At this point, the formed meniscus on the SMF has not reached the side polished fiber. In fact, the reflected optical power of the side polished fiber has not decreased and remains similar to the reflected optical power registered for air. However, in Fig. 4(a), both the SMF and side polished fiber still presents a decrease in the optical interference amplitude. This is expected for the SMF, which is now in the liquid, but it is unusual for the side polished fiber. This is unusual because the optical axis of the incident light from the optical fiber and the reflected light from the liquid surface are parallel (see Fig. 4(b)) until the SMF has reached the liquid surface. On the other hand, these two optical axes are not parallel when the meniscus forms on the SMF, as shown in Fig. 4(c). Since they are not parallel, in this instance, the Fabry-Perot interference is no longer present.

TABLE II
REFRACTIVE INDEX OF LIQUIDS (1550 NM)

Liquid	Refractive index
Deionized Water	1.32
Acetone	1.35
IPA	1.37
Ethylene Glycol	1.42
Glycerol	1.46
Mineral Oil	1.48
Diiodomethane	1.74

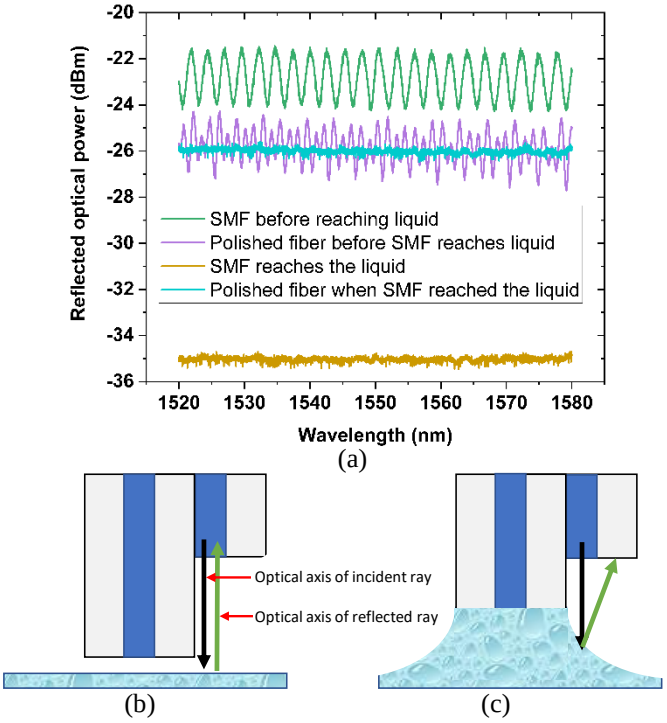

Fig. 4. Reflected optical power for both the SMF and side polished fiber before and after the SMF reaches the liquid surface (a). Depiction of the incident and reflected optical light axes light before (b) and after (c) the SMF reaches the liquid surface, respectively.

However, the reflected optical power decreases as the side polished fiber comes closer to the incoming meniscus. This could be due to some of the reflected light entering the core of the side polished fiber when the distance from the fiber and the meniscus shortens, as seen from Fig. 5(a) to Fig. 5(b). In addition, the interference amplitude increases, and it becomes more evident, as shown in Fig. 5(c), as the distance from the liquid meniscus decreases. In Fig. 5 is shown the difference of the reflected optical power interference at 2.49 and 23.2 μm distance from the incoming meniscus.

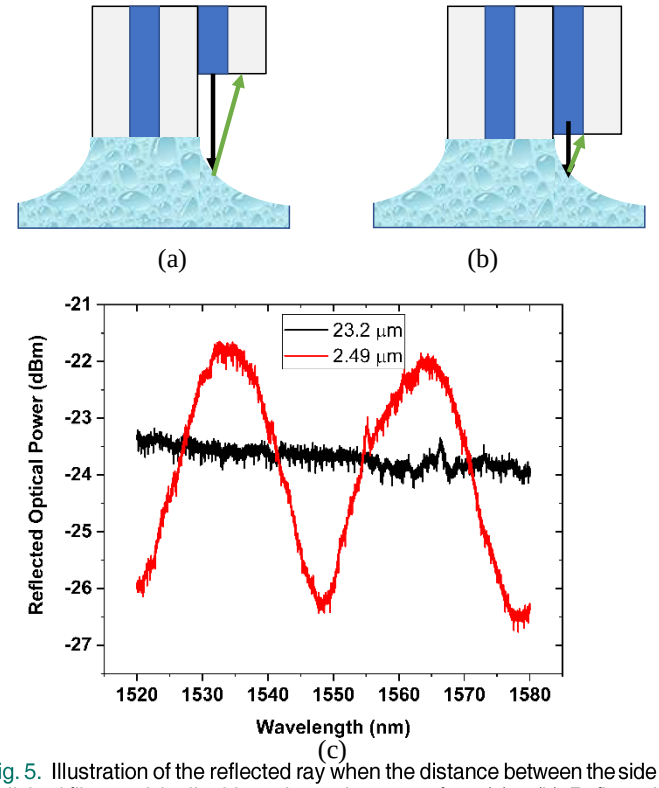

Fig. 5. Illustration of the reflected ray when the distance between the side polished fiber and the liquid meniscus decreases from (a) to (b). Reflected optical power interference at 2.49 and 23.2 μm from the incoming liquid meniscus.

In addition, a different reflection pattern profile was observed at different distances from the incoming meniscus surface of the liquid (water in this case) for the 55.0, 59.0, and 61.0 μm side polished fiber lengths. This is shown in Fig. 6, where side polished fibers with different polished lengths have the reflected light entering the optical fiber core at different distances from the incoming meniscus. For example, the most side polished fiber would result in the shortest distance between two fiber cores and therefore incur the shortest reflection distance as it reflects at a relatively higher point along the meniscus. For instance, in Fig. 6, the reflected optical power decreases at different stages. For example, the reflected optical

power seems to start decreasing at ~13.0 µm for the side polished fiber length of 55.0 µm, ~12.0 µm at 59.0 µm, and ~9.0 µm for the side polished fiber length of 61.0 µm. In addition, the start of the variation of the reflected optical power could represent a decrease of the physical dimension of the optical fiber core of the side polished fiber. Moreover, for the correct measurement of the *MH*, the height does not correspond to when the core of the optical fiber registers the first substantial variation of its reflected optical power. However, the correct measurement is equal to the point where the core of the side polished fiber is covered by the liquid, at 0.0 µm as shown in Fig. 2(d), not as shown in Fig. 2(c). In this case, the reflected optical power corresponds to the one of the liquids.

Nonetheless, the 55.0 µm polished optical fiber could present a higher error in detecting the *MH* since the meniscus could arch, as shown in [27]. On the other hand, both the 59 and 61 µm side polished fiber could be used for the analysis since the meniscus does not arch before being detected by the core of the optical fiber. However, the 61.0 µm polished optical fiber was used for measuring the *MH* since the center of the optical fiber core is closer to the surface of the SMF. Therefore, also the incident ray is closer to the SMF surface.

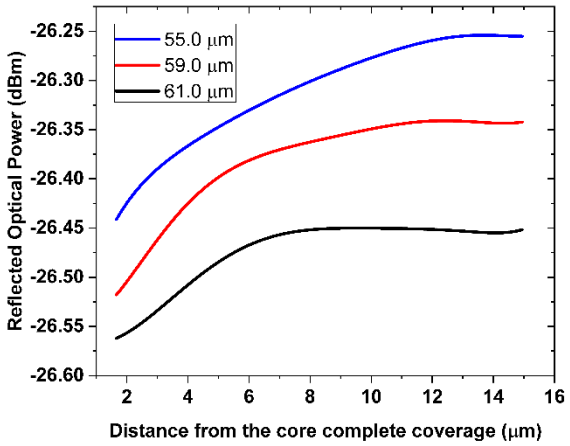

Fig. 6. Reflected optical power variation of the different side polished fiber length while the meniscus approaches the fiber.

D. Surface roughness and surface-energy

The roughness of the optical fiber, which was determined using the AFM, is 10.49±5.36 nm. This value indicates that the surface of the optical fiber is not completely smooth, as expected. In addition, the surface energy results by measuring the *MH* of water, ethylene glycol, and diiodomethane was around 50 mJ/m^2, which is higher than what can be found in currently available literature [25], possibly due to the roughness of the optical fiber cladding. This relatively high surface energy value shows that the fused silica cladding presents a high wettability for the selected liquids.

E. Contact angle measurement for surface tension

As mentioned before, the knowledge of the contact angle is needed for surface tension measurement, following (1). The static contact angle was thus measured following the procedure described in the methodology section. By obtaining the distance *D*, the contact angle was calculated by measuring the *MH*, and using James' equation. Values of the *MH* obtained are present in Fig. 7. As can be seen, *MH* changes with the selected liquid, which indicates an increase in *MH* as the surface tension decreases [28]. The contact angle for deionized water using James's equation is ~31° which corresponds to the value of water wetting a silica substrate [29]. By inserting those contact angle values in (1), the surface tension could now be determined. In Fig. 8, the calculated surface tension values and the theoretical ones are shown and compared to the theoretical results. The experimental results of the surface tension show the same tendency as the theoretical ones within the experimental standard deviation (out of 3 times measured). However, there is a slight difference between the experimental and theoretical results, which is possibly due to the low frequency of the recording data using the available interrogator, the experimental error on the *MH*, the approximation on the optical fiber to be considered as an ideal cylinder, and the fact that cleaved angle of the optical fiber tip is of 89.63 ± 0.14°, instead of 90°. In addition to this, the liquid water at room temperature absorbs wavelength radiations in the 1550 nm range, in which some light is transformed to heat [30]. Therefore, the hydrogen bonding of the liquid becomes weaker as the local heating increases [17].

In addition, with the side polished fiber attached to the SMF, the contact angle at the interface between the P3 mineral oil and water could be determined, approximating the theoretical value of 48.4 mN/m from the equation given in (4). With the present result, the Wilhelmy method was modified since the contact angle at the interface between liquid could be measured. This is because the contact angle is practically measured and not supposed to be 0°.

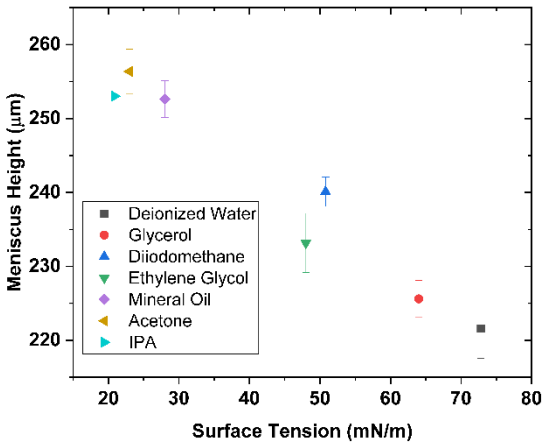

Fig. 7. Variation of the MH against the surface tension of the liquid.

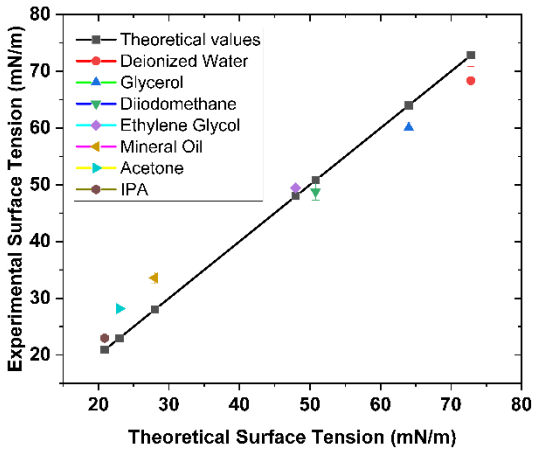

Fig. 8. Depiction of the experimental against the theoretical surface tension values of the selected liquids.

IV. Conclusion

In conclusion, the surface tension of the air-liquid and liquid-liquid interface was measured using a side polished fiber that is attached to an SMF. The sensor could be particularly used for biomedical applications since liquid-liquid interfaces are highly probable. In addition, the height of the meniscus is equal not to the first variation of the reflected optical power but to when the liquid completely covers the core of the optical fiber. Moreover, the reflected radiation is not entering the optical fiber core when the meniscus forms, and for this reason, the amplitude interface of the reflected optical power is not present. However, when the liquid moves upward, the reflected light could enter the optical fiber core, producing a variation of the reflected optical power. Nonetheless, the cleaved side polished fiber could be used as a displacement sensor since it can detect the amplitude of the reflected optical power. Future work is ongoing to examine the use of side polished fiber for measuring the height and the profile of the meniscus with other optical fiber (different materials, dimensions, and shapes) for chemical and biomedical engineering applications.

References

[1] R. Higginson, A. Parry, M. Williams, and B. Jones, "Paramedics and pneumonia associated with COVID-19," *J. Paramed. Pract.*, vol. 12, no. 5, pp. 179–185, Jul. 2020.

[2] S. Yue and D. Katabi, "Liquid testing with your smartphone," *MobiSys 2019 - Proc. 17th Annu. Int. Conf. Mob. Syst. Appl. Serv.*, pp. 275–286, Jun. 2019.

[3] Sina Ebnesajjad, "2 Surface Tension and Its Measurement," in *Surface Treatment of Materials for Adhesion Bonding*, 2006, pp. 9–28.

[4] G. S. Lapham, D. R. Dowling, and W. W. Schultz, "In situ force-balance tensiometry," *Exp. Fluids*, vol. 27, pp. 157–166, Apr. 1999.

[5] M. A. Quetzeri-Santiago, J. R. Castrejón-Pita, and A. A. Castrejón-Pita, "On the analysis of the contact angle for impacting droplets using a polynomial fitting approach," *Exp. Fluids*, vol. 61, no. 6, pp. 1–13, May 2020.

[6] P. M. Sakugawa, M. A. Jaculli, R. M. G. Santos, G. Camargo, C. E. A. G. Barreto, and H. Pedrini, "Methodology for obtaining contact angles in rock sample images using image processing and polynomial fitting techniques," *J. Pet. Explor. Prod. Technol.*, vol. 10, no. 4, pp. 1359–1366, Feb. 2020.

[7] P. Chen, Z. Policova, C. R. Pace-asciak, and A. W. Neumann, "Study of molecular interactions between lipids and proteins using dynamic surface tension measurements : a review," *Colloids Surfaces B Biointerfaces*, vol. 15, pp. 313–324, 1999.

[8] P. Chen, R. M. Prokop, S. S. Susnar, A. W. Neumann, W. Interface, and E. I. Plot, "Interfacial tensions of protein solutions using axisymmetric drop shape analysis," *Proteins Liq. Interfaces*, vol. 7, pp. 303–339, 1998.

[9] A.-G. O. M. Hasanuzzaman, A. Rafferty, M. Sajjia, "Properties of Glass Materials," in *Reference Module in Materials Science and Materials Engineering*, 2016, pp. 1–12.

[10] T. H. Nguyen, T. Venugopalan, T. Sun, and K. T. V. Grattan, "Intrinsic Fiber Optic pH Sensor for Measurement of pH Values in the Range of 0.5-6," *IEEE Sens. J.*, vol. 16, no. 4, pp. 881–887, Feb. 2016.

[11] V. A. Márquez-Cruz and J. A. Hernández-Cordero, "Fiber optic Fabry-Perot sensor for surface tension analysis," *Opt. Express*, vol. 22, no. 3, p. 3028, Feb. 2014.

[12] Y. S. Liu Zexu, Changyu Shen, Yike Xiao, Jiaqi Gong, Jianfeng Wang, Tingting Lang, Chunliu Zhao, Changqing Huang, Yongxing Jin, Xinyong Dong, Yang Zhang, Zhenguo Jing, Wei Peng, "Liquid surface tension and refractive index sensor based on a tilted fiber Bragg grating," *J. Opt. Soc. Am. B*, vol. 35, no. 6, pp. 1282–1287, May 2018.

[13] Y. Tang and S. Cheng, "The meniscus on the outside of a circular cylinder: From microscopic to macroscopic scales," *J. Colloid Interface Sci.*, vol. 533, pp. 401–408, Aug. 2019.

[14] B. B. Sauer and W. G. Kampert, "Influence of Viscosity on Forced and Spontaneous Spreading : Wilhelmy Fiber Studies Including Practical Methods for Rapid Viscosity Measurement," *J. Colloid Interface Sci.*, vol. 37, no. 199, pp. 28–37, Nov. 1998.

[15] T. Andrukh, D. Monaenkova, B. Rubin, W. K. Lee, and K. G. Kornev, "Meniscus formation in a capillary and the role of contact line friction," *Soft Matter*, vol. 10, no. 4, pp. 609–615, Nov. 2014.

[16] M. R. Rahman, A. Deng, S. A. Hussak, A. Ahmed, T. Willers, and P. R. Waghmare, "On the effect of relaxation time in interfacial tension measurement," *Colloids Surfaces A Physicochem. Eng. Asp.*, vol. 574, no. March, pp. 239–244, Apr. 2019.

[17] L. Binetti *et al.*, "Monitoring of the critical meniscus of very low liquid volumes using an optical fiber sensor," *IEEE Sens. J.*, vol. 20, no. 20, pp. 12232–12240, Jun. 2020.

[18] B. B. Sauer and N. V. Dipaolo, "Surface Tension and Dynamic Wetting of Polymers Using the Wihelmy Method : Applications to High Molecular Weights and Elevated Temperatures," *J. Colloid Interface Sci.*, vol. 144, no. 2, pp. 527–537, Jan. 1991.

[19] J. Park, U. Pasaogullari, and L. Bonville, "Wettability measurements of irregular shapes with Wilhelmy plate method," *Appl. Surf. Sci.*, vol. 427, pp. 273–280, 2017.

[20] D. F. James, "The meniscus on the outside of a small circular cylinder," *J. Fluid Mech.*, vol. 63, no. 4, pp. 657–664, Aug. 1974.

[21] J. Wang, C. A. Fuentes, D. Zhang, X. Wang, A. W. Van Vuure, and D. Seveno, "Wettability of carbon fibres at micro- and mesoscales," *Carbon N. Y.*, vol. 120, pp. 438–446, May 2017.

[22] D. Okiely, J. P. Whiteley, J. M. Oliver, and D. Vella, "Inertial rise of a meniscus on a vertical cylinder," *J. Fluid Mech.*, vol. 768, p. R2, Mar. 2015.

[23] C. Clanet and D. Quéré, "Onset of menisci," *J. Fluid Mech.*, vol. 460, pp. 131–149, Nov. 2002.

[24] V. M. Starov, "Surface forces action in a vicinity of three phase contact line and other current problems in kinetics of wetting and spreading," *Adv. Colloid Interface Sci.*, vol. 161, no. 1–2, pp. 139–152, 2010.

[25] R. Zhang and G. Azimi, "Scale-Phobic Surfaces Made of Rare Earth Oxide Ceramics," *ACS Appl. Mater. Interfaces*, vol. 12, no. 37, pp. 42339–42347, Aug. 2020.

[26] P. M. McGuiggan and J. S. Wallace, "Maximum force technique for the measurement of the surface tension of a small droplet by AFM," *J. Adhes.*, vol. 82, no. 10, pp. 997–1011, Jan. 2006.

[27] W.-J. A. de J. L. and G. de W. Wijs, "Wetting Forces and Meniscus Pinning at Geometrical Edges," *AIChE J.*, vol. 62, no. 12, pp. 4453–4465, Dec. 2016.

[28] D. Luo *et al.*, "Simultaneous measurement of liquid surface tension and contact angle by light reflection," *Opt. Express*, vol. 27, no. 12,

pp. 16703–16712, May 2019.

[29] A. L. Sumner *et al.*, "The nature of water on surfaces of laboratory systems and implications for heterogeneous chemistry in the troposphere," *Phys. Chem. Chem. Phys.*, vol. 6, no. 2, pp. 604–613, Dec. 2004.

[30] E. Preter, R. A. Katims, V. Artel, C. N. Sukenik, D. Donlagic, and A. Zadok, "Monitoring and analysis of pendant droplets evaporation using bare and monolayer-coated optical fiber facets," *Opt. Mater. Express*, vol. 4, no. 5, pp. 903–915, Apr. 2014.

Leonardo Binetti completed his bachelor's degree in Materials Science at the University of Bari, Italy, in 2015. He then successfully obtained a Masters (with Distinction) in Advanced Materials Engineering at Edinburgh Napier University, the UK, in 2018. He is currently pursuing a Ph.D. in Photonics and Surface Chemistry at Edinburgh Napier University, UK.

Lourdes Alwis obtained a first-class (Hons) degree in Electrical, Electronic and Information Engineering from City University London, UK, in 2005. She completed her Ph.D. thesis in the field of grating-based optical fiber Optic Sensors in 2013 at the same establishment while working for R&D of Alcatel-Lucent Ltd., a company specializing in design, implementation, build and test of optical fiber telecommunications products. Completing her Ph.D. and industrial experience in 2013, she joined Edinburgh Napier University, UK, as a Lecturer in Electronic Engineering. Her current research focuses on avenues where optical fiber sensors can be utilized: civil infrastructure monitoring, chemical, biomedical sensing, and wearable technology.